Inorganic Compounds as Binders for Si-Alloy Anodes

Journal of The Electrochemical Society, 2021 **168** 020505

Inorganic Compounds as Binders for Si-Alloy Anodes

Congxiao Wei[1] **and M. N. Obrovac**[1,2,*,z]

[1]*Department of Chemistry, Dalhousie University, Halifax, N. S. B3H 4R2, Canada*
[2]*Department of Physics and Atmospheric Science, Dalhousie University, Halifax, N. S. B3H 4R2, Canada*

The inorganic compounds, lithium polysilicate ($Li_2Si_5O_{11}$), sodium polyphosphate ($(NaPO_3)_n$), and lithium phosphate monobasic (H_2LiPO_4) were investigated as the sole binders in Si-alloy and graphite electrodes for Li cells. Surprisingly, the coating quality and cycling performance of Si-alloy anodes with these inorganic binders is similar to those electrodes using the state of the art lithium polyacrylate (LiPAA) organic binder. Graphite electrodes with inorganic binders show good cycling despite having poor coating quality. Graphite electrodes with lithium polysilicate binder have three times the binder volume than expected, indicating that this binder has an open framework microstructure.

 [DOI: 10.1149/1945-7111/abdc74]

Manuscript submitted November 16, 2020; revised manuscript received January 6, 2021. Published February 1, 2021.

Supplementary material for this article is available online

Lithium ion batteries are the most important energy storage devices for portable electronics and electric vehicles.[1] Si-based anodes are being investigated to improve the energy density of Li-ion batteries due to their high volumetric capacity and low average potential.[2] However, huge volume changes of Si-based materials during cycling can cause severe particle fracture and rapid solid electrolyte interphase (SEI) generation, leading to continuous Li ion consumption and cell fade.[3] Advanced binders are known to improve cycling performance and the extend cycle life of Si-based electrodes. These are usually organic polymers or molecules having a high quantity of carboxyl and hydroxyl functional groups and their alkali salts, such as poly(acrylic acid), lithium polyacrylate, sodium polyacrylate, sodium carboxymethyl cellulose, alginate, and citric acid.[4–8] Such binders are believed to work by forming ester-like covalent bonds with the surface of Si-alloys and interconnecting hydrogen bonds, that lead to the maintenance of binder-particle and particle-particle connections during cell cycling.[9–12] Nafion and its lithium counterpart, have also been shown to be effective binders for Si-alloy anodes.[13–15] Instead of carboxyl and hydroxyl functional groups, Nafion-based binders utilize sulfonic acid groups in a similar bonding mechanism with alloy surfaces. It is likely that other oxoacids or their alkali salts can also be effective binders via similar mechanisms.

Inorganic binders, such as alkali polysilicates (also commonly known as "water glass"), are commonly used as inexpensive water impermeable coatings, as binders in paint,[16] and as refractory binders.[17] Phosphates are another common class of refractory binders.[17] The structure of lithium polysilicate ($Li_2Si_5O_{11}$), sodium polyphosphate ($(NaPO_3)_n$), and lithium phosphate monobasic (H_2LiPO_4) are shown in Fig. 1a.[18,19] Such binders become hydrated when combined with water, as shown for lithium polysilicate in Fig. 1b. Lithium polysilicate, sodium polyphosphate, lithium phosphosilicate, titanium dioxide, and lithium phosphate have been reported to be effective binders for lithium manganese/iron phosphate cathode and carbon nanocomposite anodes.[20] Some good cycling results have been obtained with Si-alloy anodes using polysiloxane and organosilicate-based binders that contain organic groups.[21] To our knowledge, the use of completely inorganic binders in alloy anodes for Li-ion batteries has not been previously reported.

In this study, lithium polysilicate, sodium polyphosphate, and lithium phosphate monobasic were investigated as inorganic binders for Si-alloy and graphite anodes. These electrodes were characterized for their electrochemical performance and their microstructure was investigated before and after electrochemical cycling.

Experimental

Binders evaluated in this study were Li polysilicate (20 wt% in H_2O, Sigma-Aldrich), sodium polyphosphate (sodium hexametaphosphate, 65%–70% P_2O_5 basis, Sigma-Aldrich), and lithium phosphate monobasic (99%, Sigma-Aldrich). Two organic binders, LiPAA (used in a 10 wt.% solution, prepared by neutralizing PAA (M_w = 250,000, 35 wt.% in water, Sigma-Aldrich) with lithium hydroxide monohydrate ($LiOH \cdot H_2O$, ⩾98%, Sigma-Aldrich)) and polyvinylidene difluoride (PVDF, average $M_w \sim$ 534,000 by GPC, powder, Sigma-Aldrich), were investigated for comparison. Si alloy electrode slurries were prepared by mixing Si alloy (V7, 0.9 μm average particle size, 3M Company) and binder in a weight ratio of 9:1. N-methyl-2-pyrrolidone (NMP, Sigma-Aldrich, anhydrous 99.5%) for PVDF binder electrodes and distilled water for all other electrodes were added to control slurry viscosity. Graphite (MAGE, 20 μm average particle size, Hitachi) slurries were made using the same method. All aqueous slurries were made with the addition of ~0.1 ml isopropylene alcohol to improve wetting. Table I shows the exact coating recipe of the prepared slurries. Slurries were mixed using a high-shear mixer (Mazerustar, Kurabo Industries Ltd) at 5000 rpm for 10 min and then spread onto 15 μm thick copper foil with a 0.1 mm coating bar. All coatings were stored in air at room temperature overnight and then dried for 30 min at 120 °C in air. TiN (<3 μm, density: 5.24 g ml^{-1}, Aldrich) coatings were also prepared to measure the electrochemistry of binders without interference from an active material, as described in Ref. 10. Electrode disks with an area of 1.30 cm^2 were punched from the coatings after drying and heated under vacuum at 120 °C overnight. Then they were transferred without air exposure to an Ar-filled glovebox for cell making. The mass loadings were ~2 mg cm^{-2} and ~3 mg cm^{-2} for Si-alloy and graphite electrodes, respectively, corresponding to specific capacities of and ~2.4 mAh cm^{-2} and ~1.1 mAh cm^{-2}, respectively.

Coin cell assembly was carried out in an Ar-filled glove box. 2325 coin cells were made with a working electrode vs Li metal foil (99.9%, trace metals basis, Sigma-Aldrich) as a counter/reference electrode. 1M $LiPF_6$ (battery grade from BASF) dissolved in a 3:6:1 by volume solvent mixture of ethylene carbonate: diethyl carbonate: fluoroethylene carbonate (all battery grade from BASF) was used as electrolyte. Two layers of Celgard-2301 and one layer of polypropylene blown microfiber separator (BMF, ~190 μm thick, from 3M Company) were used as separators. BMF was utilized as a

*Electrochemical Society Member.
zE-mail: mnobrovac@dal.ca

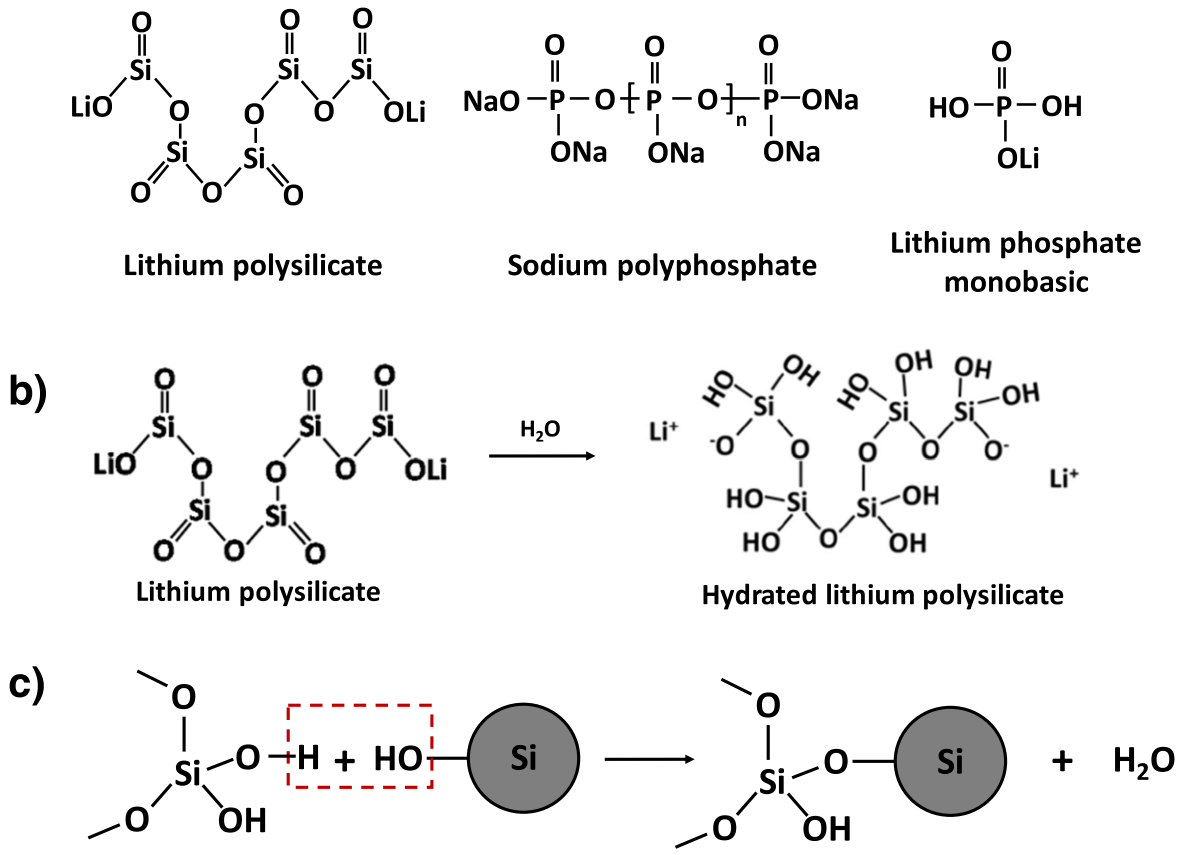

Figure 1. (a) Structures of the inorganic binders investigated in this study. (b) Mechanism showing the lithium polysilicate conversion to hydrated lithium polysilicate in water. (c) Proposed mechanism of how hydrated lithium polysilicate forms bonds with Si-alloy particle surfaces.

Table I. Slurry formulations for the electrode coatings prepared in this study.

Slurry		Solids (wt.% of total solids)			Liquids (g)		
		Si-alloy	Graphite	Binder	Isopropanol	H_2O	NMP
Binder 10 wt%	$Li_2Si_5O_{11}$	90		10	0.089	1.0	—
			90	10	0.089	1.5	—
	$(NaPO_3)_n$	90		10	0.089	1.0	—
			90	10	0.089	1.5	—
(0.89 g solids)	H_2LiPO_4	90		10	0.089	1.0	—
			90	10	0.089	1.5	—
	LiPAA	90		10	0.089	1.0	—
	PVDF	90		10	—	—	1.1
Binder 20 wt%	$Li_2Si_5O_{11}$		80	20	0.10	1.7	—
	$(NaPO_3)_n$		80	20	0.10	1.7	—
(1.0 g solids)	H_2LiPO_4		80	20	0.10	1.7	—

separator to improve stack pressure distribution and reduce electrode edge effects in coin cells, as described in a previous study.[22] Celgard 2301 separator was utilized in conjunction with the BMF separator to reduce lithium dendrite formation. Each Li-ion cell contained two Cu spacers (total thickness of 1.5 mm) to provide proper internal pressure.

Coin cells were tested using a Maccor Series 4000 Automated Test System and cycled between potential limits of 0.005–0.9 V for the first two cycles with a C/10 and a C/40 trickle discharge at 0.005 V and following cycles with a rate of C/5 and a C/20 trickle discharge at 0.005 V. Pristine and post-cycled Si-alloy and graphite electrodes were cross-sectioned in a plane parallel to their thickness direction by ion milling with Ar^+ ions using a cross-section polisher (JEOL, IB-19530CP). The cross-sectional plane was imaged using a scanning electron microscope (SEM, TESCAN MIRA3) with an accelerating potential of 5 kV. To abate air exposure, a desiccator was used to transfer cycled electrode samples to the cross-section polisher, and a stream of argon gas was flowed over the post-cycled electrodes during the sample loading procedure for the cross-section polisher and SEM. Binder true density was measured using a Micromeritics AccuPyc II 1340 gas pycnometer with a dry helium atmosphere.

Results and Discussion

Alloy electrodes prepared using inorganic binders resulted in well-adhered and homogeneous coatings as shown in Figs. 2a–2c. We ascribe the good mechanical properties of these coatings to the

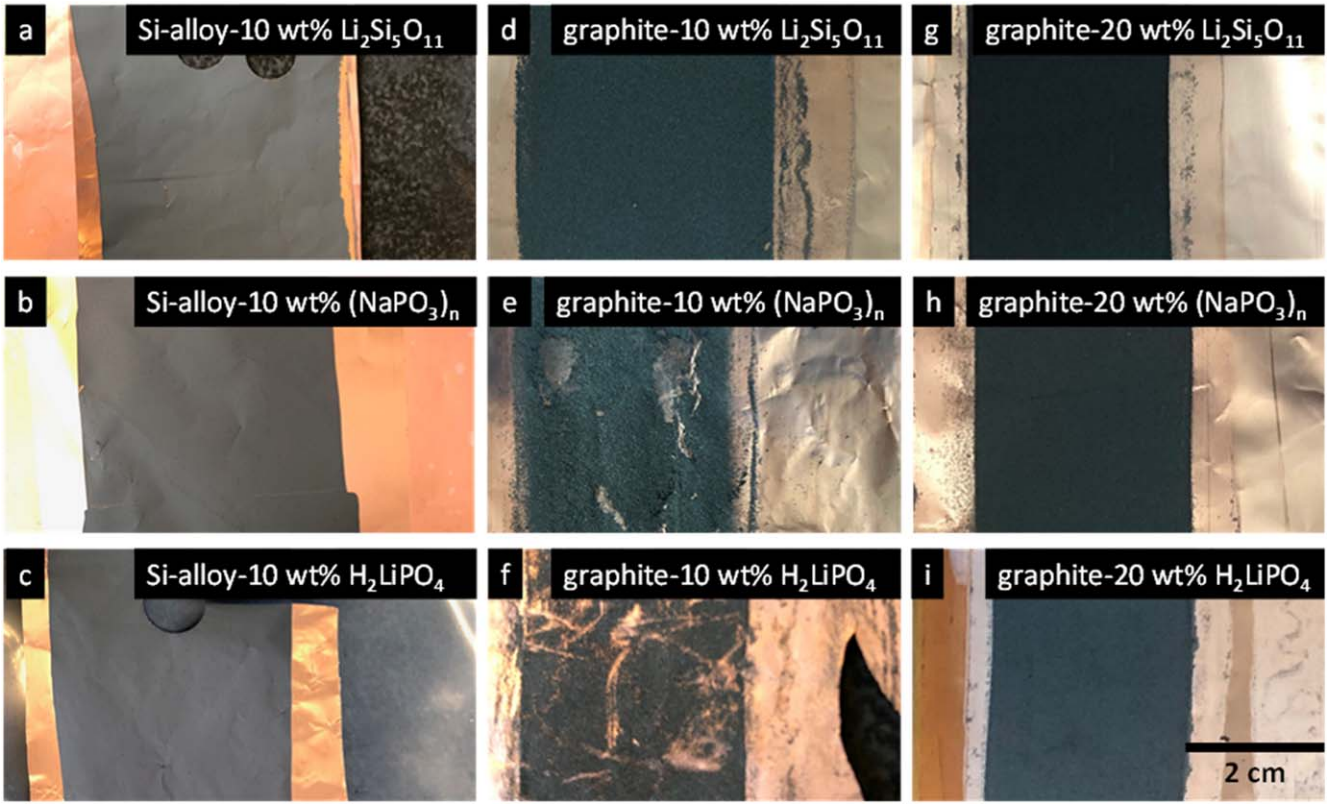

Figure 2. Digital photographs of (a)–(c) Si alloy and (d)–(i) graphite coatings prepared with $Li_2Si_5O_{11}$, $(NaPO_3)_n$, and H_2LiPO_4 binders, as indicated.

ability of hydroxyl groups on hydrated inorganic binders to react with the hydroxyl groups on the Si-alloy surface and form Si-O-Si bonds, as shown in Fig. 1c. This is similar to the mechanism of bond formation between alloy surfaces and binders containing carboxyl groups, discussed in the introduction. In contrast, poor electrode integrity resulted when the binder was used with graphite, which has no surface functionality that can form bonds with the binders. This resulted in binder solution separation from the graphite particles during the coating process. Due to the low viscosity of the aqueous electrode slurry and no binder-graphite bonding, the graphite particles settled quickly, while the binder solution continued to spread laterally on the Cu foil. As a result, the amount of binder remaining in the dried coated electrode was low. Portions of the coating sloughed off from the electrodes when electrodes were punched. This solids/liquid separation was especially severe for the LiH_2PO_4 coating, in which white LiH_2PO_4 crystals were observed on the Cu foil surface at the sides of the coating after drying. Given the poor quality of these graphite coatings with 10 wt% binder (see Figs. 2d–2f), graphite coatings were remade with a higher binder fraction of 20 wt% in order to increase the binder fraction in the dried coating and improve mechanical characteristics, so that the electrodes could be more successfully incorporated into electrochemical cells. As can be seen in Figs. 2g–2i, graphite electrode quality was significantly improved by increasing the binder fraction. Adding thickeners or other binders to increase slurry viscosity and improve the coating mechanical integrity may be required when such binders are used with graphite. However, the use of thickeners was avoided in this study, since thickeners (e.g. CMC) also have carboxylic acid groups, which would alter cycling performance. Here, the performance of the pure binders only was of interest.

Electrodes comprised of TiN and binder were prepared to study binder electrochemistry. TiN is electrically conductive and electrochemically inert at low potentials. For this reason, binder electrochemical performance can be examined in a composite coating without interference from active materials.[10] Figure 3 shows the first cycle potential curves of LiPAA, $Li_2Si_5O_{11}$, $(NaPO_3)_n$, and H_2LiPO_4 binders in TiN/binder electrodes where the TiN/binder weight ratio is 9/1, corresponding to a TiN/binder volume ratio of 73/27, 80/20, 81/19, and 79/21 for the TiN/LiPAA, TiN/$Li_2Si_5O_{11}$, TiN/$(NaPO_3)_n$, and TiN/H_2LiPO_4 electrodes, respectively. The volume fraction of each electrode component was obtained based on the densities listed in Table II. The initial lithiation capacities of LiPAA, $Li_2Si_5O_{11}$, $(NaPO_3)_n$, and H_2LiPO_4 are 180, 201, 307, and 411 mAh g^{-1} respectively, and the first cycle reversible capacities are 55, 53, 87, and 69 mAh g^{-1} respectively. The first lithiation capacity of $Li_2Si_5O_{11}$ is slightly higher than LiPAA. The $(NaPO_3)_n$, and H_2LiPO_4 first lithiation capacities are significantly higher than LiPAA, possibly because of the incomplete removal of water with the drying conditions used. The large first lithiation capacity of H_2LiPO_4 binder may be a result of it being the only protic binder tested. This would lead to the reduction of H^+ during the first lithiation to generate H_2. After the first lithiation, all binders tested were electrochemically inactive, with small first lithiation and reversible capacities (~25 mAh g^{-1}) compared to active binders, such as polyimide (1943 mAh g^{-1} first lithiation and 874 mAh g^{-1} reversible capacity).[10]

Figure 4 shows the first cycle potential vs capacity curves for Si-alloy electrodes with inorganic binders and with commonly-used LiPAA organic binder. In commercial cells, alloys are blended with graphite to reduce volume expansion and improve cycling performance.[2] Here, electrodes, with 100% alloy as the active material and containing no carbon black, represent an extreme test for binder performance. All potential profiles are similar and show a nucleation plateau at ~0.16 V and two characteristic sloping plateaus of Si.[25] Electrodes with inorganic binders have a higher first lithiation capacity and higher irreversible capacity than the electrode with LiPAA, while reversible capacities were similar. The reversible capacities of the Si-alloy electrodes with $Li_2Si_5O_{11}$, $(NaPO_3)_n$, H_2LiPO_4, and LiPAA binders, were 1122 mAh g^{-1}, 1128 mAh g^{-1}, 1032 mAh g^{-1}, and 1167 mAh g^{-1}, respectively.

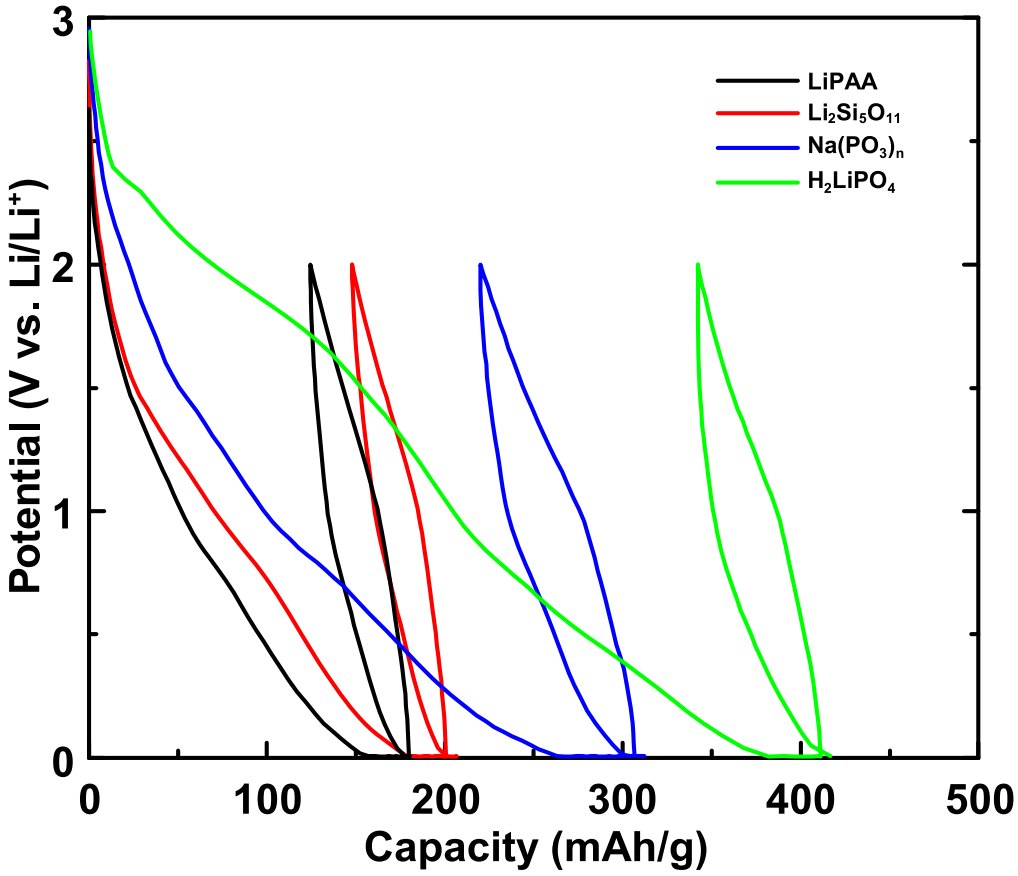

Figure 3. Potential profiles of LiPAA, $Li_2Si_5O_{11}$, $(NaPO_3)_n$, and H_2LiPO_4 binders vs Li-metal as measured in TiN/binder composite coatings.

Table II. Densities of electrode component materials in g cm^{-3}.

	TiN	LiPAA	$Li_2Si_5O_{11}$	$(NaPO_3)_n$	H_2LiPO_4	MAGE
Density	5.24	1.54[23]	2.27[24]	2.52	2.16	2.26[23]

The initial coulombic efficiency (ICE) values of the electrodes with $Li_2Si_5O_{11}$, $(NaPO_3)_n$, H_2LiPO_4, and LiPAA binders, were 80%, 79%, 74%, and 86%, respectively. The lowest ICE value is that of the Si-alloy/H_2LiPO_4 electrode, as expected from the TiN/H_2LiPO_4 electrode performance discussed above.

Figures 5a–5d shows the capacity and coulombic efficiency (CE) vs cycle number of the Si-alloy electrodes with (a) PVDF organic binder and (b)–(d) inorganic binders. The CEs are not plotted for the electrode with PVDF binder since its capacity fade was so high as to render its CE meaningless. The capacity vs cycle number is also shown for an Si-alloy electrode with LiPAA organic binder, which is typically utilized for state-of-the-art Si-alloy electrodes, for comparison. Duplicate cells were used to confirm the electrochemical performance. In Fig. 5 capacity is shown in terms of percent capacity retention (with respect to the reversible capacity). Corresponding plots of specific capacity vs cycle number are shown in Fig. S1 (available online at stacks.iop.org/JES/168/020505/mmedia). Si-alloy electrodes with PVDF binder lost almost all their capacity after the first cycle. Such catastrophic failure is expected in this extreme electrode formulation for unfunctionalized binders, such as PVDF, because of the absence of chemical bonds between PVDF and Si-alloy surfaces.[26–28] It has also been recently shown that the poor cycling of PVDF electrodes can also be attributed to its reactivity with lithiated Si.[29]

In contrast to the poor performance of PVDF binder, all of the inorganic binders tested have excellent performance in this extreme Si-alloy electrode formulation. The cycle 2–100 capacity retention of the Si-alloy/LiPAA, Si-alloy/$Li_2Si_5O_{11}$, Si-alloy/$(NaPO_3)_n$, and Si-alloy/H_2LiPO_4 electrodes tested were 80.65% 71.75%, 81.05%, and 82.56%, respectively. The capacity retention and CE of the Si-alloy/$(NaPO_3)_n$ and Si-alloy/H_2LiPO_4 electrodes are essentially identical to that of the Si-alloy/LiPAA electrode. Slightly more capacity fade and lower CE values were observed for the Si-alloy/$Li_2Si_5O_{11}$ electrode. Despite their good cycling performance, the reproducibility of cells with Si-alloy/H_2LiPO_4 electrodes was poor (see Fig. S1d). This is likely due to gas formation during cycling from the reduction of H^+. In addition, electrode slurries made from H_2LiPO_4 had low viscosity, resulting in powder settling and the binder solution bleeding out the sides of the coating after casting. The good cycling performance of these binders is highly surprising for brittle inorganic species that are not expected to be able to accommodate alloy volume expansion during cycling. However, LiPAA is also brittle. It has been suggested that PAA binders form an effective artificial SEI layer that is responsible for the good cycling characteristics of alloy electrodes with PAA binder.[6] However, this explanation is difficult to reconcile with the fact that alloys undergo significant surface erosion, in which the alloy surface is completely destroyed and disrupted during cycling. This will be discussed further below. Graphite electrodes using 10 wt.% or 20 wt.% inorganic binder all had good electrochemical performance, as shown in Figs. 5e, 5f. This is despite the poor quality of some of these electrodes. The first charge capacity values

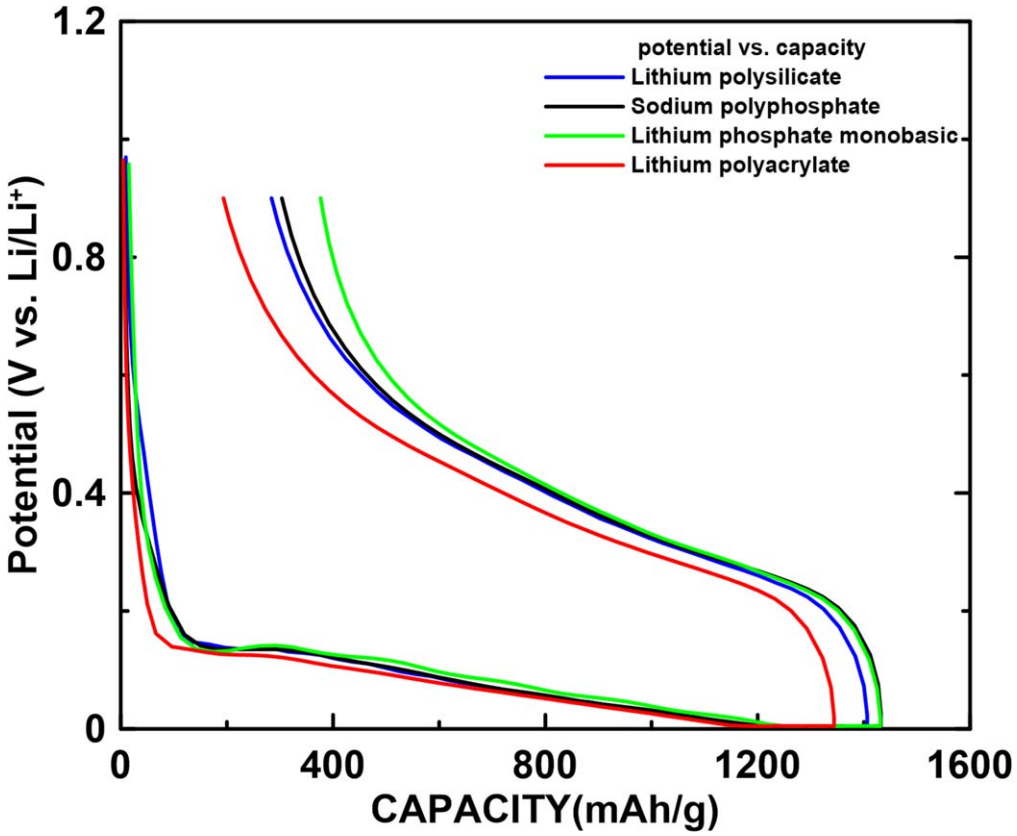

Figure 4. The first cycle potential vs capacity curves of Si-alloy electrodes with $Li_2Si_5O_{11}$, $(NaPO_3)_n$, H_2LiPO_4, and LiPAA binders.

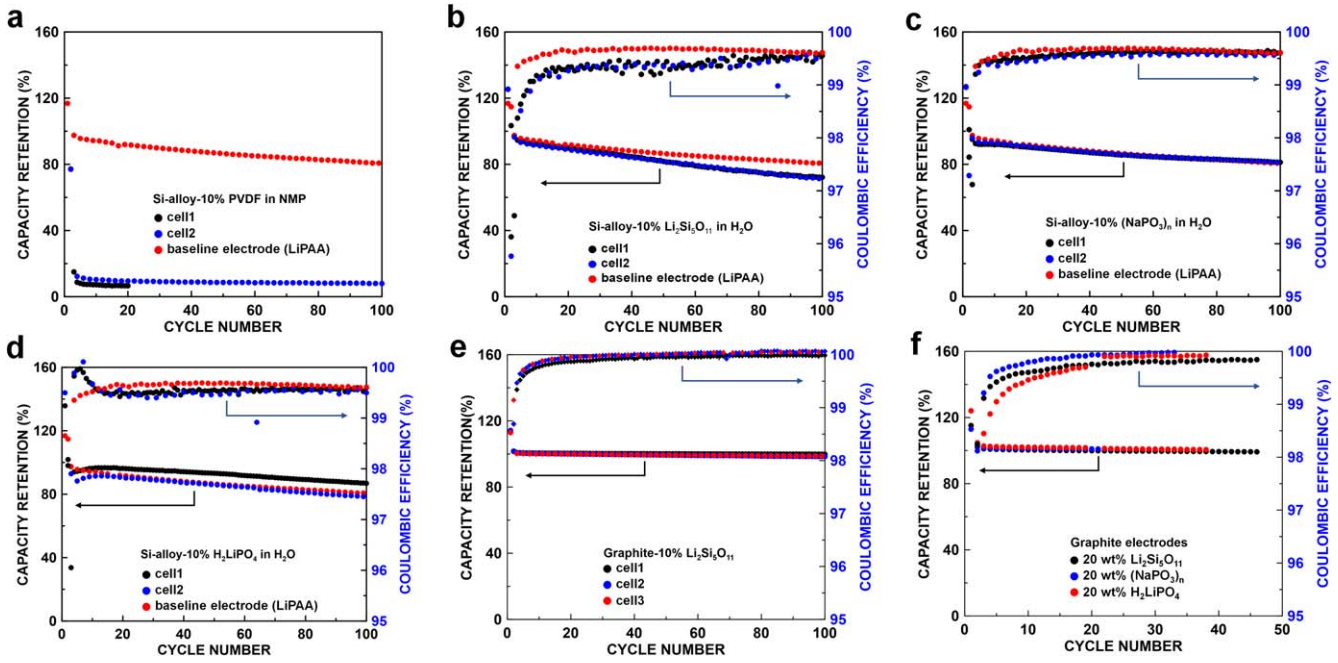

Figure 5. Discharge capacity and CE vs cycle number of (a) Si-alloy with PVDF and LiPAA conventional binders (CE not shown), (b) Si-alloy/$Li_2Si_5O_{11}$, (c) Si-alloy/$(NaPO_3)_n$, (d) Si-alloy/H_2LiPO_4, (e) graphite/$Li_2Si_5O_{11}$, and (f) graphite/20 wt% inorganic binder electrodes.

of graphite electrodes with 20 wt% of $Li_2Si_5O_{11}$, $(NaPO_3)_n$, and H_2LiPO_4 binders, were 367 mAh g^{-1}, 368mAh g^{-1}, and 363 mAh g^{-1}, respectively. However, the inability of these inorganic binders to provide mechanical association with graphite results in fragile coatings that are not practical to handle. Again, the use of thickeners may solve this issue.

Figure 6 shows the morphology of electrode cross sections before and after cycling of the same Si alloy electrodes whose performance is shown in Fig. 5 (excepting the PVDF electrode, whose morphology was the same before and after cycling, as this electrode essentially did not function). After 100 cycles, the surface of the alloy particles in all these electrodes was severely eroded. This

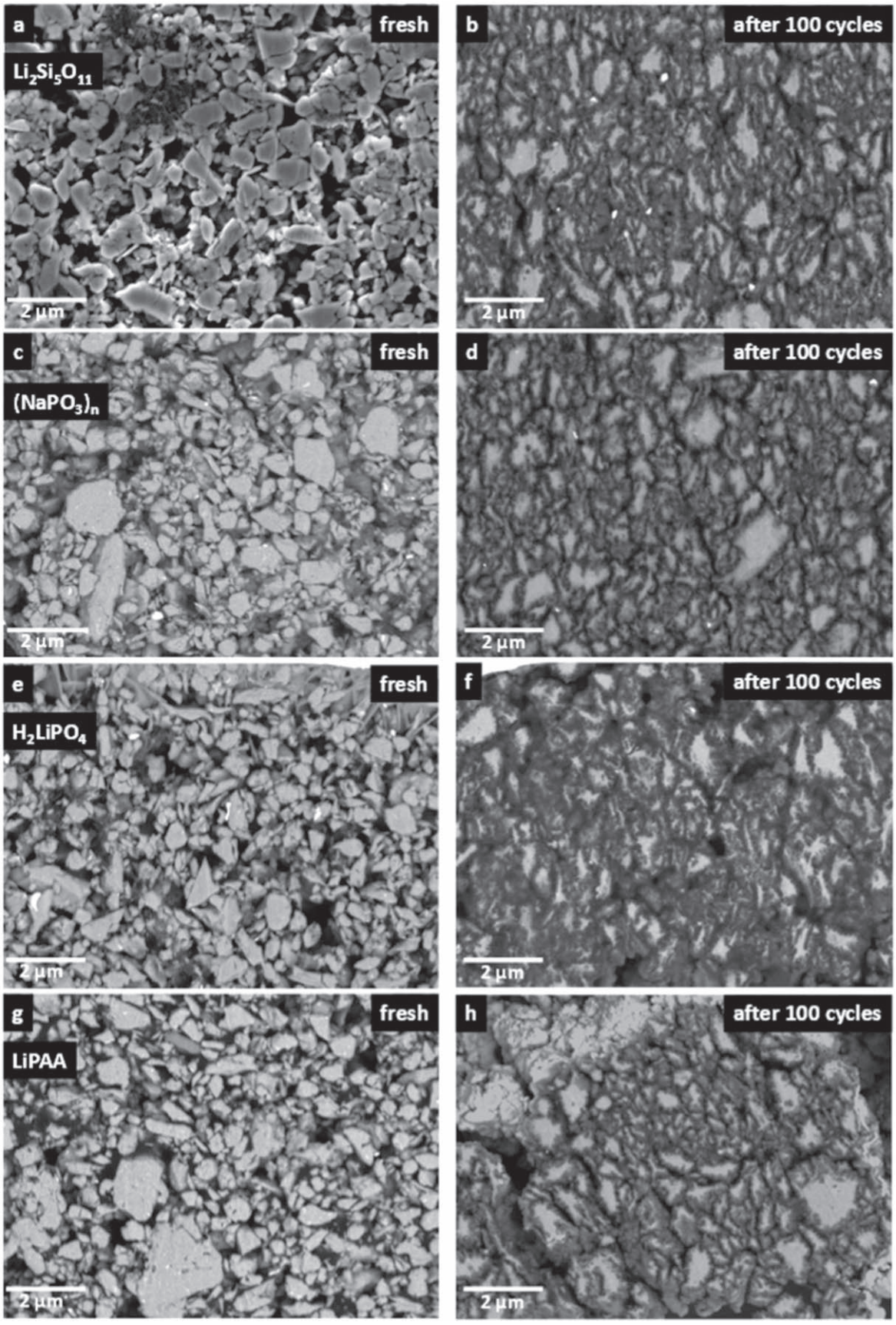

Figure 6. SEM images of (a), (c), (e), (g) pristine and (b), (d), (f), (h) post-cycled (100 cycles) Si-alloy/$Li_2Si_5O_{11}$, Si-alloy/$(NaPO_3)_n$, Si-alloy/H_2LiPO_4, and Si-alloy/LiPAA electrodes, respectively.

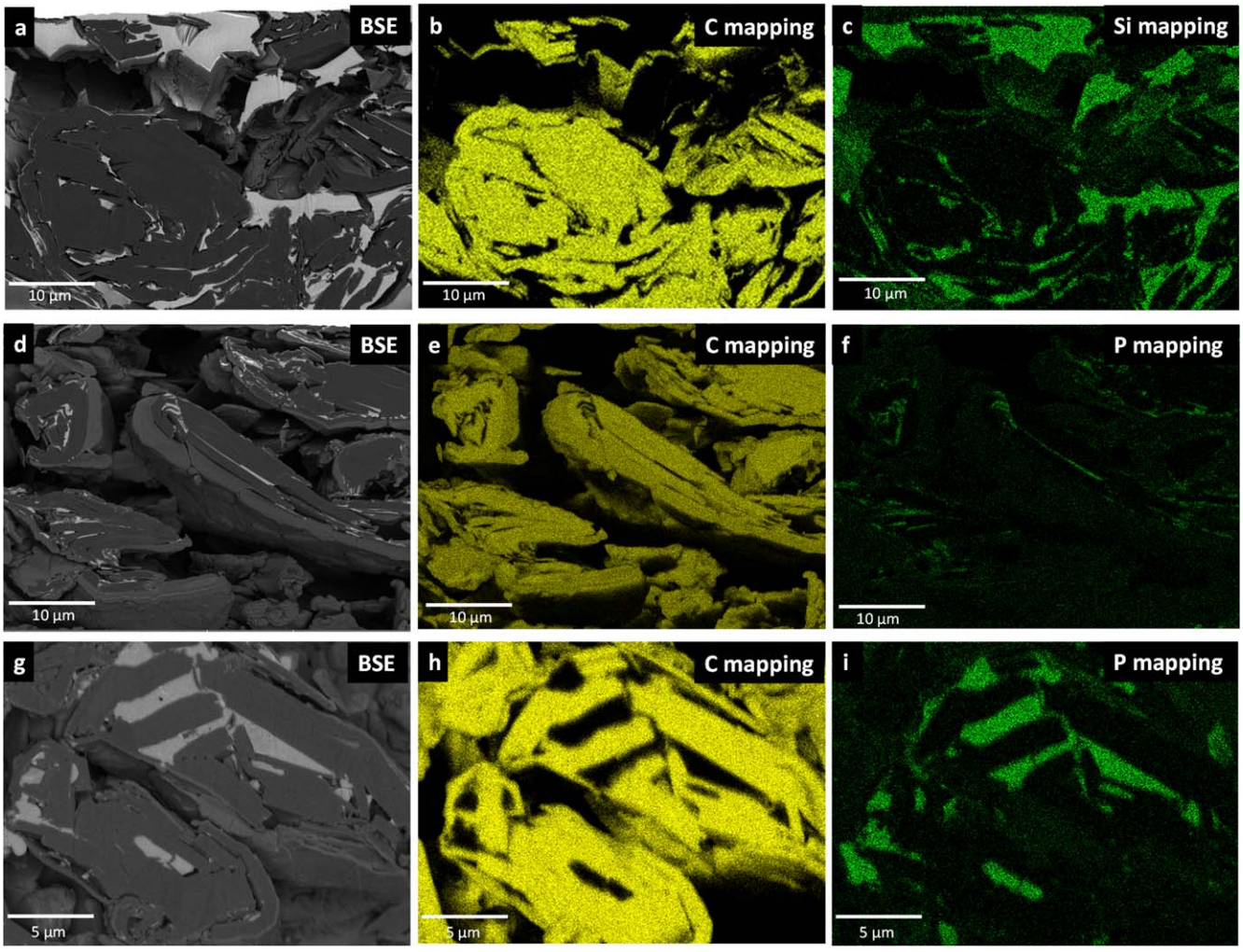

Figure 7. (a), (d), (g) BSE, (b), (e), (h) C mapping, and (c), (f), (i) Si/P mapping of pristine graphite/$Li_2Si_5O_{11}$, graphite/$(NaPO_3)_n$, and graphite/H_2LiPO_4 electrodes, respectively.

results in submicron alloy fragments breaking off from the original alloy particles and reacting with the electrolyte to form a submicron alloy/SEI composite. This is seen as a grey halo surrounding still pristine alloy particle cores in the SEM images. This effect has been seen previously for Si-alloy electrodes with LiPAA binder.[30] Such surface erosion increases the alloy surface area, resulting in parasitic reactions with the electrolyte.[30] However, in half-cells such reactions do not necessarily result in capacity fade.[31] Indeed, even though most of the alloy of the Si-alloy/H_2LiPO_4 electrode has been eroded away after 100 cycles, the capacity retention remains similar to LiPAA. Therefore, the submicron alloy fragments that result from the erosion of the alloy surface must remain electrochemically active. It is difficult to believe that the binder, which makes up such a small volume fraction of these coatings could possibly be forming an effective "artificial SEI layer" on all the submicron alloy fragments that are formed or that the binder could possibly be providing a "healing" effect, as suggested in previous binder studies, when the alloy has mostly disintegrated. Therefore, the question as to how carboxylate binders (or the inorganic binders described in this manuscript) can function despite the near total disintegration of the active phase in some cases remains unanswered in our opinion.

Figure 7 shows cross-sectional backscattered electron (BSE) images and element mappings of graphite electrodes using $Li_2Si_5O_{11}$, $(NaPO_3)_n$, and H_2LiPO_4 binders. These images show that these inorganic binders can enter into voids inside the graphite particles during the electrode slurry making process. This was confirmed by elemental mapping of the electrodes. Little binder actually appeared on outer surfaces of the graphite particles, which can explain the observation that these binders fail to physically hold graphite particles mechanically. The large volume fraction taken up by the $Li_2Si_5O_{11}$ binder is remarkable. Figure 8 shows the theoretical (based on the

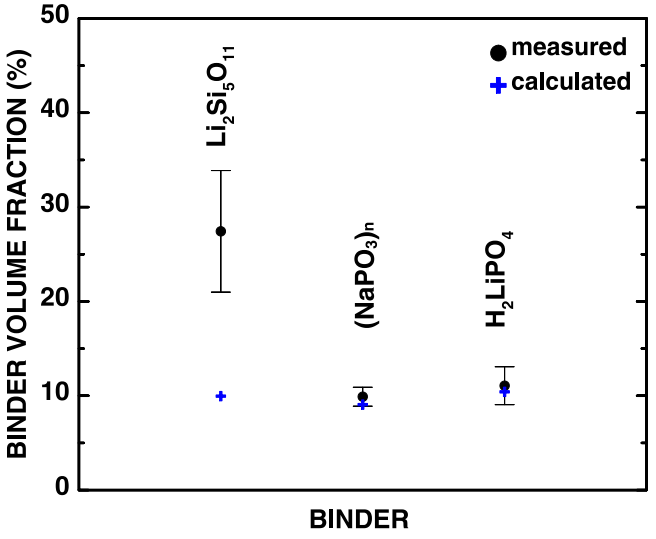

Figure 8. Theoretical and measured inorganic binder volume fractions in graphite/binder (10 wt%) electrodes.

electrode formulation and the component densities in Table II) and measured inorganic binder volume fractions in graphite electrodes (as observed in SEM cross-section images). The error bars in the measured values represent differences between multiple SEM images acquired from each electrode. The measured binder volume fractions of both $(NaPO_3)_n$ and H_2LiPO_4 electrodes are in good agreement with the theoretical binder fractions (~10%). However, the $Li_2Si_5O_{11}$ electrode has an observed binder fraction that is nearly three times greater than the theoretical value.

The above results suggest that the $Li_2Si_5O_{11}$ binder likely has an open structure, similar to a sol-gel. Considering that electrodes with $Li_2Si_5O_{11}$ cycle with little fade at near theoretical capacity, it is apparent that the large volume of binder must allow ion diffusion. This suggests that $Li_2Si_5O_{11}$ binder is likely in the form of a porous gel that is filled with electrolyte. We believe that this represents a new class of binders that has not been explored. Interestingly $Li_2Si_5O_{11}$ did not form such gels when used with a Si-alloy anode, as shown in Fig. 6a. This may be because, in contrast to when it is used with graphite, $Li_2Si_5O_{11}$ can bond directly to the alloy surface and therefore tends to wet the surface rather than aggregate into regions of porous gel.

Conclusions

In this work, three inorganic binders, $Li_2Si_5O_{11}$, $(NaPO_3)_n$, and H_2LiPO_4, were implemented in Si-alloy and graphite electrodes. They have poor adhesion to graphite, however, resulting in graphite coatings that cycle well, but have poor mechanical properties. Increasing binder amount was found to improve the graphite coating quality. Adding thickeners or other binders to increase slurry viscosity and improve the coating mechanical integrity may be required when inorganic binders are used with graphite. In graphite coatings, lithium polysilicate binder was observed to take up an area that is much larger than can be accounted for by the amount used. We ascribe this to the formation of a gel that can be filled with electrolyte, allowing ion conduction. We believe that this represents a new class of binder.

Si-alloy electrodes with these inorganic binders had both excellent mechanical properties and cycling performance; as good as electrodes made with state-of-the-art LiPAA binder. This implies that the silicic and phosphoric acid groups are just as effective as carboxylic acid groups thought responsible for LiPAA's good performance. These binders represent a brand-new approach for achieving good cycling in Si-alloy electrodes.

Acknowledgments

The authors acknowledge financial support from NSERC, Novonix, the Canada Foundation for Innovation, and the Atlantic Innovation Fund for this work. Congxiao Wei would like to thank Dr. Xiang Yang at Saint Mary's University for his assistance in acquiring SEM images.

ORCID

M. N. Obrovac https://orcid.org/0000-0001-5509-3185

References

1. G. E. Blomgren, *J. Electrochem. Soc.*, **164**, A5019 (2017).
2. M. N. Obrovac and V. L. Chevrier, *Chem. Rev.*, **114**, 11444 (2014).
3. M. N. Obrovac, L. Christensen, D. B. Le, and J. R. Dahn, *J. Electrochem. Soc.*, **154**, A849 (2007).
4. A. Magasinski, B. Zdyrko, I. Kovalenko, B. Hertzberg, R. Burtovyy, C. F. Huebner, T. F. Fuller, I. Luzinov, and G. Yushin, *ACS Appl. Mater. Interfaces*, **2**, 3004 (2010).
5. S. Komaba, N. Yabuuchi, T. Ozeki, Z. J. Han, K. Shimomura, H. Yui, Y. Katayama, and T. Miura, *J. Phys. Chem. C*, **116**, 1380 (2012).
6. Z. Karkar, D. Guyomard, L. Roué, and B. Lestriez, *Electrochim. Acta*, **258**, 453 (2017).
7. I. Kovalenko, B. Zdyrko, A. Magasinski, B. Hertzberg, Z. Milicev, R. Burtovyy, I. Luzinov, and G. Yushin, *Science (80-.)*, **334**, 75 (2011).
8. C. C. Nguyen, D. M. Seo, K. W. D. K. Chandrasiri, and B. L. Lucht, *Langmuir*, **33**, 9254 (2017).
9. W. Porcher, S. Chazelle, A. Boulineau, N. Mariage, J. P. Alper, T. Van Rompaey, J.-S. Bridel, and C. Haon, *J. Electrochem. Soc.*, **164**, A3633 (2017).
10. B. N. Wilkes, Z. L. Brown, L. J. Krause, M. Triemert, and M. N. Obrovac, *J. Electrochem. Soc.*, **163**, A364 (2015).
11. J. S. Bridel, T. Azas, M. Morcrette, J. M. Tarascon, and D. Larcher, *J. Electrochem. Soc.*, **158**, A750 (2011).
12. D. Munao, J. W. M. Van Erven, M. Valvo, E. Garcia-Tamayo, and E. M. Kelder, *J. Power Sources*, **196**, 6695 (2011).
13. R. R. Garsuch, D. B. Le, A. Garsuch, J. Li, S. Wang, A. Farooq, and J. R. Dahn, *J. Electrochem. Soc.*, **155**, A721 (2008).
14. Y. Wang, D. Dang, D. Li, J. Hu, X. Zhan, and Y. T. Cheng, *J. Power Sources*, **438**, 226938 (2019).
15. J. Xu, L. Zhang, Y. Wang, T. Chen, M. Al-Shroofy, and Y. T. Cheng, *ACS Appl. Mater. Interfaces*, **9**, 3562 (2017).
16. D. Stoye and W. Freitag, *Paint, Coatings and Solvents* (WILEY-VCH, Federal Republic of Germany) 2nd ed. (1998).
17. S. Banerjee, *Monolithic Refractories: A Comprehensive Handbook* (World Scientific Publishing Co. Pte. Ltd., Singapore) (1998).
18. D. Wendel, D. Reiter, A. Porzelt, P. J. Altmann, S. Inoue, and B. Rieger, *J. Am. Chem. Soc.*, **139**, 17193 (2017).
19. H. F. W. Taylor, *J. Am. Ceram. Soc.*, **69**, 464 (1986).
20. A. Kay, *US Patent Application*, US20110117432A1 (2011).
21. D. A. Shariaty, D. Qian, Y.-T. Cheng, and S. A. Odom, *J. Electrochem. Soc.*, **165**, A731 (2018).
22. Z. Yan and M. N. Obrovac, *J. Electrochem. Soc.*, **164**, A2977 (2017).
23. Z. Du, R. A. Dunlap, and M. N. Obrovac, *J. Electrochem. Soc.*, **161**, A1698 (2014).
24. B. Tischendorf, C. Ma, E. Hammersten, P. Venhuizen, M. Peters, M. Affatigato, and S. Feller, *J. Non. Cryst. Solids*, **239**, 197 (1996).
25. D. S. M. Iaboni and M. N. Obrovac, *J. Electrochem. Soc.*, **163**, A255 (2016).
26. S. Komaba, K. Shimomura, N. Yabuuchi, T. Ozeki, H. Yui, and K. Konno, *J. Phys. Chem. C*, **115**, 13487 (2011).
27. D. Mazouzi, Z. Karkar, C. R. Hernandez, P. J. Manero, D. Guyomard, L. Roué, and B. Lestriez, *J. Power Sources*, **280**, 533 (2015).
28. T. W. Kwon, J. W. Choi, and A. Coskun, *Chem. Soc. Rev.*, **47**, 2145 (2018).
29. B. Han, M. J. Piernas-Muñoz, F. Dogan, J. Kubal, S. E. Trask, I. D. Bloom, J. T. Vaughey, and B. Key, *J. Electrochem. Soc.*, **166**, A2396 (2019).
30. L. J. Krause, T. Brandt, V. L. Chevrier, and L. D. Jensen, *J. Electrochem. Soc.*, **164**, A2277 (2017).
31. V. L. Chevrier, L. Liu, D. B. Le, J. Lund, B. Molla, K. Reimer, L. J. Krause, L. D. Jensen, E. Figgemeier, and K. W. Eberman, *J. Electrochem. Soc.*, **161**, A783 (2014).